RSC Applied Interfaces

ROYAL SOCIETY OF CHEMISTRY

PAPER

View Article Online
View Journal | View Issue

Cite this: *RSC Appl. Interfaces*, 2026, 3, 500

Study on electrical contact of a solid–liquid interface between a copper-based electrode and liquid metal

Jiasheng Zu,[ab] Yuntao Cui, *[a] Chunwei Li,[ab] Xueqing Chen[ab] and Zhongshan Deng *[ab]

Copper-based electrodes are widely used for electrical connections due to their excellent electrical and thermal conductivity. However, efficient electrical connectivity is often hindered by high interfacial contact resistance and reliability issues inherent in conventional solid–solid contacts. Gallium-based liquid metals (GLMs) offer a solution through their unique liquid-state compliant contact and reactive interface. This study systematically investigates the reactive wetting behavior and electrical contact stability of GLM in contact with four common copper-based electrode types: pure copper (T2), brass (H62), bronze (QSn6.5-0.1), and alumina-dispersed copper (C15760). Contact resistance at the solid–liquid interface was measured quantitatively using the transmission line model method. The results demonstrate that contact resistance undergoes a progressive reduction and reaches a quasi-steady state after 20 days of continuous contact. This is primarily due to enhanced interfacial wettability and the consequent increase in the effective contact area. Notably, the T2 and H62 interfaces achieved a stable contact resistivity of approximately 10^{-6} Ω cm^2. Microstructural analysis (XRD and SEM) confirms the formation of a $CuGa_2$ intermetallic compound layer through reactive wetting. This intermetallic compound layer significantly enables a transition from discrete physical contact to a stable, metallic bond wetting, thereby effectively reducing solid–liquid contact resistance. These findings demonstrate the great potential of gallium-based liquid metal for forming reliable and efficient solid–liquid electrical contacts with copper-based electrodes *via* reactive wetting. This opens broad prospects for advanced electrical interface applications.

Received 25th November 2025,
Accepted 26th January 2026

DOI: 10.1039/d5lf00370a

rsc.li/RSCApplInter

1. Introduction

The rapid development of high-speed railways,[1] ultra-high-voltage transmission and substation equipment,[2] and high-power electronic devices[3] has surged the demand for electrical connections with superior reliability and stability. In critical components such as photovoltaic connectors,[4] conductive slip rings,[5] and electrical switching devices,[6] maintaining a low and consistent contact resistance over service periods is paramount. However, conventional solid–solid electrical contact interfaces possess intrinsic microscopic surface roughness, which severely constrains the actual contact area to a fraction of the nominal surface. This results in constriction resistance and compromised connection stability and reliability.[7] Poor electrical contact between solid conductors increases resistance, leading to the Joule heating effect and accelerating device degradation, and reducing service life.

Reducing contact resistance and enhancing interfacial stability are crucial to addressing these challenges and developing next-generation electrical contact technologies. Copper-based electrodes are widely used as conductors due to their excellent conductivity. Various connection methods, such as crimping, plugging, brazing, and soldering, are employed to expand the effective contact area to mitigate resistance. Nonetheless, each method has its limitations. For example, soldering processes involve high temperatures that can damage conductors and induce significant thermal stress,[8,9] while plugging typically requires substantial insertion force to ensure a secure connection.[10]

Gallium-based liquid metals have emerged as an attractive alternative due to their non-toxicity, superior electrical and thermal conductivity, and unique metallic fluidity.[11] These materials have demonstrated promising performance in a variety of applications, including flexible electronics,[12] self-healing electrodes,[13,14] soft robotics,[15] RF switches,[16] electrocatalysis,[17] electro-actuators,[18] memristors,[19]

[a] State Key Laboratory of Cryogenic Science and Technology, Technical Institute of Physics and Chemistry, Chinese Academy of Sciences, Beijing 100190, China. E-mail: cuiyuntao@mail.ipc.ac.cn, zsdeng@mail.ipc.ac.cn
[b] School of Future Technology, University of Chinese Academy of Sciences, Beijing 100049, China

supercapacitors[20] and electromagnetic shielding.[21] Integrating liquid metal with solid conductors can result in notably low contact resistance and stable electrical connections. For instance, Ozutemiz *et al.*[22] leveraged the intrinsic wettability between liquid metal and copper to achieve seamless integration of eutectic gallium–indium (EGaIn) with copper-clad stretchable circuits. Similarly, Li *et al.*[23] developed a high-power-capacity RF switch utilizing liquid metal as wetted contacts, achieving a total contact resistance below 0.05 Ω. Sarfo *et al.*[24] demonstrated that a Cu–Galinstan–Cu system could sustain a low contact resistance of 0.057 mΩ for 12 hours under a 250 A current. Liquid metals have proven effective in establishing reliable interfacial contacts with diverse functional materials, including carbon nanotubes,[25] graphene,[26] solderable patches,[27] and even biological tissues such as nerves.[28]

Although liquid metal electrodes have demonstrated excellent performance in various electronic components, further research is imperative to quantify the magnitude, interfacial composition, and influencing factors of contact resistance at solid–liquid interfaces. The transmission line model (TLM) method has effectively adapted to measure contact resistance between EGaIn and copper, achieving milliohm-level accuracy.[29–31] Previous studies mostly focused on the wetting behavior and intermetallic formation of liquid metal and planar pure copper. In industrial applications, various cylindrical copper conductors are often used to meet specific electrical connection requirements. The existing literature lacks further clarification on the interface interaction between different cylindrical copper electrodes and liquid metals in solid–liquid electrical contact, as well as the relationship between contact resistance and time variation. Given that practical electrical contact behavior (specifically, contact resistance and stability) is dictated by a complex interplay of the geometry of the conductor, contact pressure, and surface conditions,[32] it is therefore crucial to have a comprehensive understanding of the underlying interfacial mechanisms of solid–liquid interfacial interactions.

The interfacial behavior and contact resistance between liquid metal and four representative copper alloys (T2, H62, QSn6.5-0.1, and C15760) are systematically investigated in this study. Contact resistance at the solid–liquid interface was measured using the TLM method and analyzed in relation to reactive wetting and contact resistance. X-ray diffraction (XRD) and scanning electron microscopy (SEM) were utilized to characterize the interfacial transformations. The results demonstrated the formation of a reactive $CuGa_2$ alloy layer at the interface, which significantly enhanced wettability and reduced contact resistance, thereby improving the overall electrical connection stability. This study presents a surface engineering strategy based on reactive wetting to mitigate interfacial resistance in copper–liquid metal systems, providing a foundation for the development of reliable electrical contact technologies.

2. Experimental section

2.1 Experimental materials

The liquid metal used in this study was eutectic gallium–indium (EGaIn), prepared by melting high-purity gallium (99.99%) and indium (99.99%) in a weight ratio of 75.5 : 24.5 at 200 °C. The mixture was stirred for 30 minutes to ensure that it was homogeneous. Four types of commercial copper-based electrodes were investigated. Their nominal compositions (wt%) are as follows: (1) T2 (pure copper): Cu ≥ 99.9%; (2) H62 (brass): 60.5–63.5% Cu and 36.5–39.5% Zn; (3) QSn6.5-0.1 (bronze): 6.0–7.0% Sn and 0.1% P (phosphorus), balance Cu; (4) C15760 (dispersion strengthened copper): 0.58–0.62% Al (present as dispersed Al_2O_3 nanoparticles), balance Cu.

Cylindrical copper-based electrodes with a diameter of 1.0 mm were used for measuring contact resistance. The initial surface roughness (R_a) of four different types of copper electrodes is as follows: 1.501 μm (T2), 1.539 μm (H62), 1.374 μm (QSn6.5-0.1), and 1.711 μm (C15760). Prior to testing, all electrodes were ultrasonically cleaned in ethanol for 5 minutes each to remove organic contaminants. Custom 3D-printed molds were fabricated *via* stereolithography (SLA) on a Formlabs Form 3 printer using 8200 photopolymer resin (refer to Fig. 3e for structural details). The internal cavity is rectangular, with dimensions of 64 mm × 3 mm × 3.6 mm. Additionally, there are small holes with a diameter of 1 mm in the side walls of the mold, and the center-to-center spacing between adjacent holes is 3, 5, 7, 9, 11, and 13 mm, respectively. For comparative analysis under various filling conditions, flat electrodes (50 mm × 0.5 mm × 0.2 mm) were used for total resistance evaluation. Electrical contact grease (Kunlun 801, PetroChina Lubricants Company) was used for comparison purposes during testing. A UV curable adhesive (Kafuter K-3001) is used for sealing test samples.

2.2 Characterization

The static contact angles between the gallium-based liquid metal (EGaIn) and the four copper-based electrodes were measured using a JC2000D contact angle goniometer (Shanghai Zhongchen Digital Technology) *via* the sessile drop method. A 1.0 M HCl solution was prepared by diluting analytical grade concentrated hydrochloric acid with deionized water. For the static contact angle tests, all measurements were conducted at room temperature. The EGaIn droplets were dispensed and measured while completely submerged in the HCl solution. To ensure consistency, a droplet volume of 5 μL was dispensed for each measurement. Images were captured at a resolution of 1400 × 600 pixels. A stabilization period of 60 s was maintained to ensure initial equilibrium. Static contact angles were extracted using ImageJ software equipped with the DropSnake plugin, which employs the Snake approach. This geometric fitting method was chosen to accommodate the slight non-spherical deformations induced by the oxide skin, enabling the independent determination of left and right

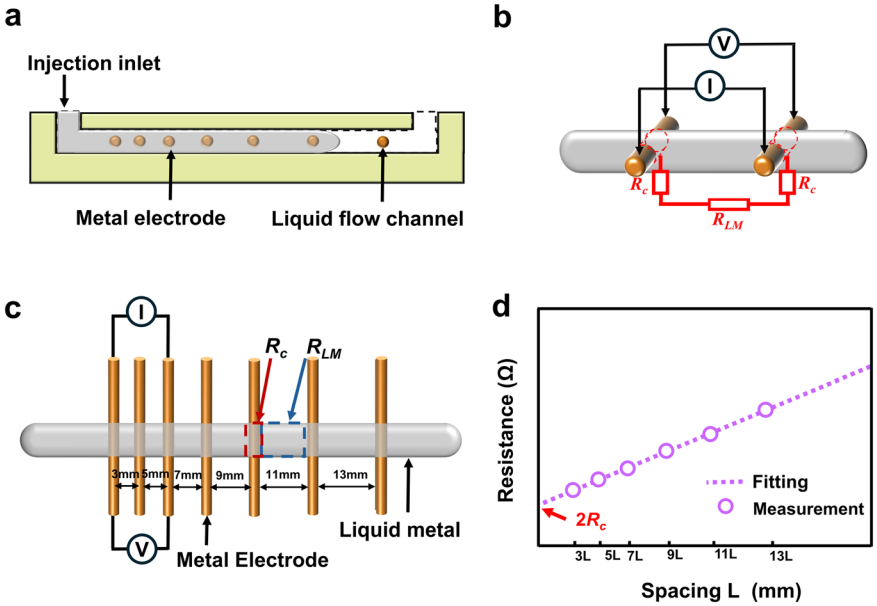

Fig. 1 (a) Schematic diagram of the sample measurement unit assembly; (b) the four-wire method used to measure the total resistance of a solid–liquid electrode pair; (c) the principle of measuring solid–liquid contact resistance based on the transmission line model; (d) schematic illustration of the data processing and fitting for measurement analysis.

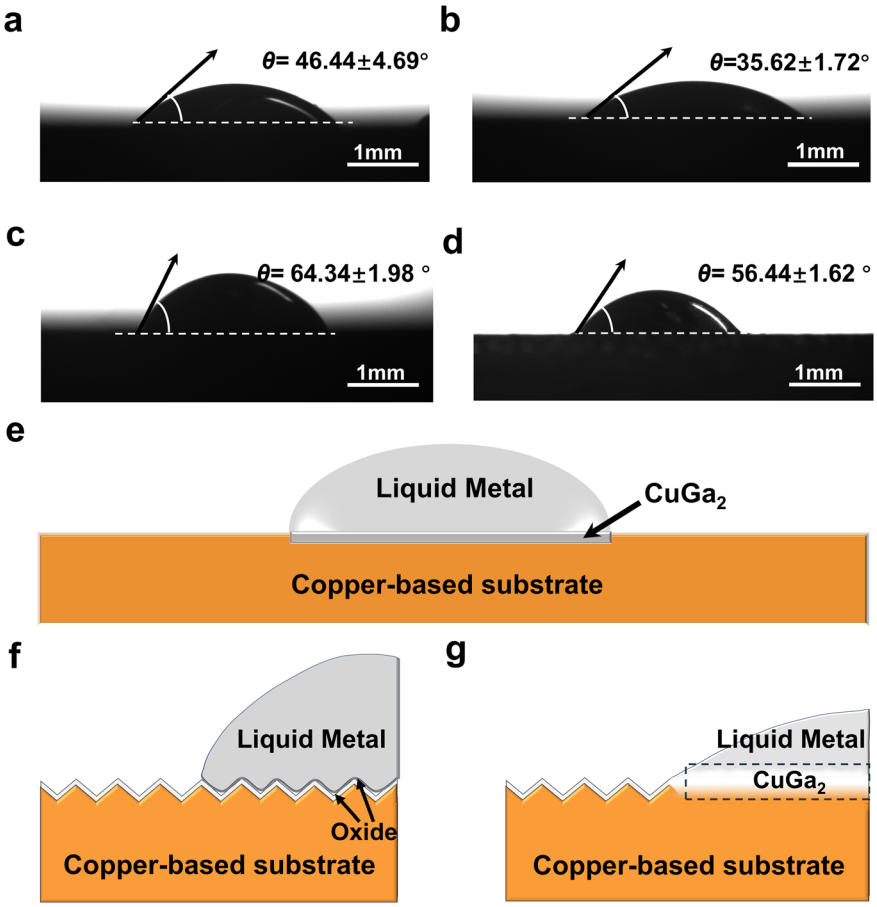

Fig. 2 The solid–liquid contact angles of four copper-based electrodes with liquid metal in 1 M HCl solution: (a) T2; (b) H62; (c) QSn6.5-0.1; (d) C15760. (e) Schematic illustration of the wetting mechanism between the liquid metal and copper-based electrodes. (f and g) Microscopic schematic illustrations of the solid–liquid contact interface as the contact time increases.

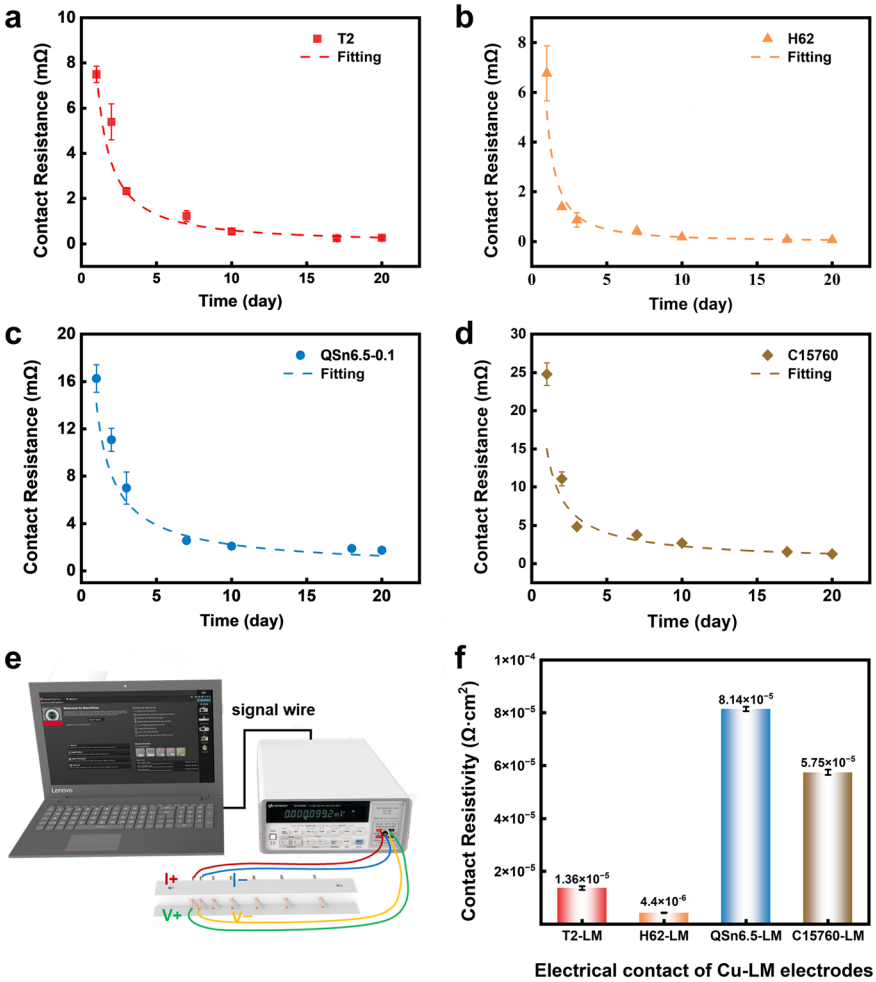

Fig. 3 The variation in solid–liquid contact resistance for four copper-based electrodes in contact with liquid metal as a function of measurement time: (a) T2; (b) H62; (c) QSn6.5-0.1; and (d) C15760. (e) The solid–liquid contact resistance measurement system. (f) The corresponding contact resistance values after 20 days.

contact angles. For each material, at least four independent measurements were performed for each substrate, and the average values with standard deviations were reported.

Electrical resistance was measured at room temperature using a 34420A precision digital multimeter (Agilent Technologies, USA) with a four-wire Kelvin configuration to eliminate lead resistance. The experimental configuration of contact resistance measurement is shown in Fig. 1c. The phase evolution of the electrode surfaces after 0 days and 20 days of continuous contact was analyzed by X-ray diffraction (XRD, Bruker D8 Focus, Germany) using Cu Kα radiation (λ = 0.15418 nm). The surface morphology and elemental distribution were further investigated using field-emission scanning electron microscopy (FE-SEM, Quanta 250 FEG, FEI, USA) with energy-dispersive X-ray spectroscopy (EDS).

2.3 Transmission line model

The measurement unit consisted of a liquid metal electrode, copper-based electrodes, and a custom 3D-printed mold. The internal channel of the mold, fabricated from photopolymer resin, was designed to accommodate the liquid metal electrode with dimensions of 64 mm × 3 mm × 3.6 mm (length × width × height). Lateral circular ports were horizontally arranged along the resin chamber to house the copper-based electrodes, with precise center-to-center spacings of 3, 5, 7, 9, 11, and 13 mm. During assembly, the electrodes were sequentially inserted into these ports, followed by the injection of liquid metal into the channel *via* a syringe to ensure air-free filling. Both the channel ends and the electrode–mold junctions were hermetically sealed using a UV-curable adhesive to prevent leakage and air infiltration.

As illustrated in Fig. 1a, the copper-based electrodes were perpendicularly inserted into the lateral holes to establish electrical contact with the liquid metal in the central channel. The total resistance (R_T) for each solid–liquid electrical contact pair was measured at various electrode spacings using a four-wire Kelvin method (Fig. 1b). To ensure measurement accuracy, voltage and current sources were applied to both sides of the copper-based electrodes, effectively eliminating their own resistance from measurement (Fig. 1c).[29] In this TLM configuration, total

resistance (R_T) consists of the bulk resistance of the liquid metal (R_{LM}) and twice the contact resistance (R_c) at the interface between the liquid metal and the copper-based electrode. The data fitting and extraction process for R_c is schematically illustrated in Fig. 1d. All experimental conditions were repeated at least three times ($N = 3$). Results are reported as mean ± standard deviation.

As described above, the total resistance (R_T) can be calculated by

$$R_T = R_{LM} + 2R_c \quad (1)$$

where R_T is the total measured resistance (Ω), R_{LM} is the bulk resistance of the liquid metal (Ω), and R_c is the contact resistance at the solid–liquid interface (Ω).

The bulk resistance of liquid metal (R_{LM}) is given by:

$$R_{LM} = \alpha L_{LM} \quad (2)$$

where $\alpha = \rho/A$, ρ is the resistivity of liquid metal (Ω m), A is the cross-sectional area of the liquid channel (m^2), and L_{LM} is the distance between two copper-based electrodes (m).

The contact resistivity (ρ_c) is calculated as:

$$\rho_c = R_c S \quad (3)$$

where R_c is the measured contact resistance (Ω) and S is the contact area between the copper-based electrode and the liquid metal (cm^2).

The extraction of contact resistance (R_c) *via* the TLM method is predicated on the assumption of a quasi-uniform current distribution across the interface.[30,33] While three-dimensional current crowding effects can occur at the edges of liquid metal–solid metal contacts due to their comparable conductivities, the high linearity of the R_T *vs.* L_{LM} plots ($R^2 > 0.95$) in our experiments confirms that such geometric effects are consistent and do not compromise the validity of the results within this experimental configuration. Furthermore, the accuracy is further ensured by the four-wire Kelvin configuration, which isolates the interfacial resistance from the bulk resistance of the measurement circuitry.

3. Results and discussion

The contact resistance between the liquid metal and copper-based electrodes is influenced by many factors, including electrode geometry, surface roughness, wetting, and contact duration. Of these factors, wetting has a significant impact on the effective contact area, thereby affecting electrical performance and reliability. According to Holm's contact resistance model,[34] the interface contact resistance between two conductors is directly proportional to the material resistivity and inversely proportional to the contact area. Therefore, when establishing an electrical connection between a copper-based electrode and liquid metal, the contact area at the solid–liquid interface plays a critical role in determining the contact resistance.

Before evaluating the electrical contact performance, the wetting behavior between the copper-based electrodes and EGaIn was evaluated. Static contact angles (θ) were measured using the sessile drop method under 1.0 M HCl immersion to ensure the removal of surface oxides, as shown in Fig. 2a–d (images were captured 60 s after contact). The measured contact angles for T2, H62, QSn6.5-0.1, and C15760 were 46.44 ± 4.69°, 35.62 ± 1.72°, 64.34 ± 1.98°, and 56.44 ± 1.62°, respectively. These values signify favorable wetting ($\theta < 90°$) across all four copper-based substrates, with a wettability sequence of H62 > T2 > C15760 > QSn6.5-0.1. The underlying solid–liquid wetting mechanism and microscopic interfacial evolution are depicted in Fig. 2e–g. Upon contact, surface Cu atoms undergo a spontaneous reaction with the Ga atoms at room temperature, forming an intermetallic compound layer of $CuGa_2$.[35] The primary role of indium is to act as a solvent to lower the melting point of gallium, forming a eutectic alloy (EGaIn) that maintains its fluid characteristics at room temperature. Although In is essential for maintaining the eutectic liquidity of EGaIn, it remains relatively inert at the interface. Thermodynamic analysis confirms that the Ga–Cu interaction exhibits a significantly stronger chemical affinity compared to In–Cu, rendering Ga the primary driver for oxide penetration and subsequent reactive wetting.[36–38] The formation of the $CuGa_2$ intermetallic layers facilitates a fundamental transition of the interface from discrete physical contact to a state of metallic bond wetting.[39] The delocalized electrons in the $CuGa_2$ intermetallic layer create a continuous electronic pathway, significantly lowering the solid–liquid interfacial energy (γ_{SL}) and thereby enhancing wettability (reducing the contact angle).[40,41]

The distinct wettability observed among the copper alloy electrodes can be attributed to their varying surface chemistry. For the T2 electrodes, the high Cu content increases the probability of contact between Cu and Ga atoms per unit area, accelerating the reactive wetting process. Similarly, the H62 electrode exhibits the lowest contact angle due to its significant Zn content (36.5–39.5%). Much like Cu, Zn possesses a strong chemical affinity for Ga,[42] which further facilitates the spread of liquid metal. In contrast, QSn6.5-0.1 and C15760 contain phosphorus (P) and alumina (Al_2O_3), both of which are known to have poor wettability with the liquid metal. These components may partially inhibit wetting to some extent, thereby reducing the effective contact area between the liquid metal and the electrodes. These factors account for the wettability differences among the four copper-based materials. Overall, however, all four copper-based electrodes demonstrate favorable liquid metal wettability ($\theta < 90°$). This not only facilitates liquid metal spreading and increases the effective solid–liquid contact area but also provides a critical foundation for improving electrical contact performance.

Fig. 3a–d show the evolution of the contact resistance at the solid–liquid interface over a period of 20 days, with the corresponding measurement configuration illustrated in Fig. 3e. Within the first 24 hours of contact, the contact resistance R_c for T2, H62, QSn6.5-0.1, and C15760 in contact with the liquid metal ranged from 1.93 to 8.11 mΩ. Notably, the T2–EGaIn and H62–EGaIn solid–liquid interfaces exhibited relatively low R_c compared to QSn6.5-0.1–EGaIn and C15760–EGaIn. After three days, all electrodes showed a marked reduction in contact resistance, signifying a rapid improvement in interfacial electrical contact. As the contact time increased, the R_c of all four electrodes progressively converged toward a quasi-steady state. By the 20th day, a clear trend towards minimal resistance was observed. The order of contact resistance among the four copper-based electrodes was as follows: H62–EGaIn < T2–EGaIn < C15760–EGaIn < QSn6.5-0.1–EGaIn, with H62–EGaIn exhibiting the lowest value.

The observed decrease in contact resistance with increasing contact time can be explained by the following factors. Initially, the presence of self-limiting nanoscale oxide films on both the liquid metal and copper-based electrode acts as a formidable barrier to wetting. This barrier leads to the formation of interfacial voids, which severely constrict the effective contact area and manifest an increase in contact resistance (see Fig. 2e). As contact time increases, the oxide film undergoes localized spontaneous rupture, enabling direct atomic-level interaction between the liquid metal and the surface of the copper-based electrode. Once this oxide barrier is compromised, it facilitates a reactive wetting process that significantly enhances the wettability and spreading of the liquid metal on the electrode surface.[43] Electron microscopic analysis (see Fig. S1a–d) confirms that, after 20 days of contact, a continuous and dense tetragonal $CuGa_2$ intermetallic compound layer is established across all four copper-based electrode surfaces. This layer is formed by Ga atoms diffusing into the copper substrate and Cu atoms migrating into the liquid phase. The presence of the $CuGa_2$ layer enhances the effective contact area by improving surface wettability. More importantly, it establishes robust metallic bonding at the interface. This provides an efficient pathway for free electrons to traverse the entire interface, facilitating unobstructed electron transport across the solid–liquid boundary.[39,44] Consequently, the $CuGa_2$ intermetallic compound layer essentially acts as an "electronic bridge" at the interface, greatly enhancing interfacial electron transfer efficiency and significantly reducing the solid–liquid contact resistance (see Fig. 2g). In time-sensitive applications, pre-treatment with HCl solution can accelerate electrode and liquid metal wetting, shortening contact resistance stabilization timescales and optimizing high-power interconnect efficiency.

Fig. S2 shows the total resistance measurements for the four copper-based electrodes after 20 days in contact with liquid metal. A strong linear relationship was observed between the measured total resistance (R_T) and the spacing between the electrodes (L_{LM}) for each pair of electrode–liquid metal. To facilitate a clearer comparison among the four copper-based electrodes, the contact resistivity (ρ_c) was calculated by multiplying the measured contact resistance (R_c) by the nominal contact area ($S = 9.42 \times 10^{-2}$ cm^2). The resulting contact resistivities, calculated according to eqn (3), are summarized in Fig. 3f. The calculated ρ_c values for the T2, H62, QSn6.5-0.1, and C15760 electrodes in contact with the liquid metal were $1.36 \pm 0.04 \times 10^{-5}$ Ω cm^2, $4.4 \pm 0.01 \times 10^{-6}$ Ω cm^2, $8.14 \pm 0.09 \times 10^{-5}$ Ω cm^2, and $5.75 \pm 0.07 \times 10^{-5}$ Ω cm^2, respectively.

These results clearly indicate that the contact resistivity of copper-based electrodes in electrical contact with the liquid metal is affected by both the intrinsic resistivity of the conductor and the contact resistance at the solid–liquid interface. The conductivity of the four copper-based electrodes is given in Table S1. Notably, the magnitude of the contact resistance for each electrode correlates strongly with its wettability: lower contact angles (*i.e.*, better wettability) consistently correspond to lower contact resistances. Therefore, improving the wettability at the solid–liquid interface directly increases the effective contact area, which significantly reduces the contact resistance and improves the stability of the electrical connection.

Fig. 4 shows the XRD patterns of the four copper-based electrodes after 0 and 20 days of contact with the liquid metal. In this study, "0 days" refers to approximately one hour of contact time. Fig. 4a demonstrates the formation of a $CuGa_2$ alloy layer on the T2 electrode surface after 20 days, as indicated by diffraction peaks that correspond to the $CuGa_2$ phase in addition to those of the T2 phase. This intermetallic compound $CuGa_2$ layer significantly facilitates the spreading of the liquid metal across the copper-based substrate, enlarging the effective solid–liquid contact area. Similarly, after 20 days, diffraction peaks associated with the $CuGa_2$ phase also appeared on the QSn6.5-0.1 and C15760 electrodes, though the $CuGa_2$ peak intensity was less pronounced in C15760 than in the QSn6.5-0.1 sample (see Fig. 4c and d). For the H62 electrode (see Fig. 4b), the diffraction peaks corresponding to the $CuGa_2$ phase were notably more pronounced than those of the H62 phase itself after 20 days. Following contact with the liquid metal, diffraction peaks corresponding to the $CuGa_2$ phase appeared on all four copper-based electrodes, with the intensity in the following order: H62 > T2 > QSn6.5-0.1 > C15760. Fig. S4 clearly illustrates the $CuGa_2$ alloy layers formed on these electrodes after interaction with the liquid metal. Notably, this observed peak intensity sequence aligns well with the wettability ranking of the four copper-based electrodes as stated above. This correlation suggests that a more pronounced $CuGa_2$ phase at the electrode interface is closely linked to enhanced solid–liquid wettability.

The micrometer-sized $CuGa_2$ layer observed in the study serves as a key "electron bridge", transitioning the liquid–solid interface from physical contact to metal bonding, fundamentally achieving ultra-low contact resistance. In

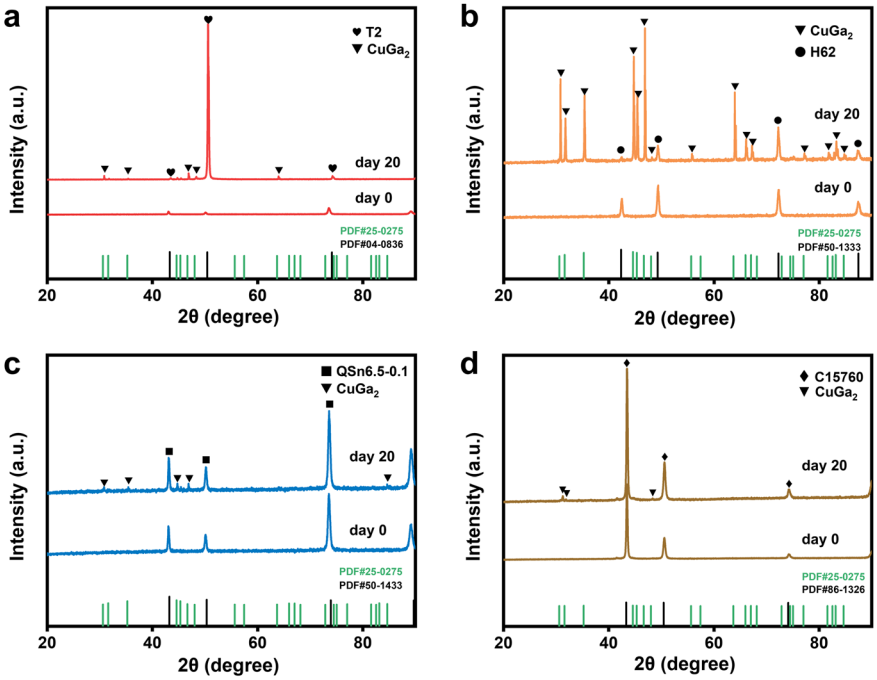

Fig. 4 XRD patterns of the four copper-based electrodes after contact with the liquid metal at day 0 and day 20: (a) T2; (b) H62; (c) QSn6.5-0.1; (d) C15760.

theory, the bulk resistance of intermetallic compounds with thicker film layers will increase accordingly, but compared to the significant decrease in contact resistance, the contribution of micrometer-thin $CuGa_2$ layers to the total resistance can be ignored.

In addition, the growth of this layer is controlled by diffusion-controlled kinetics, following the parabolic rate law, where the growth rate decreases over time.[36] This self-limiting behavior prevents the risk of losing control at room temperature. From a dynamic perspective, there exists an "optimal thickness" range: the layer must be thick enough to ensure continuous coverage of maximum wetting between the liquid and solid, but thin enough to avoid the formation of voids. The stable resistance values observed within 20 days indicate that the interface is still in this functional state.

Previous studies have indicated that the wetting ability of gallium-based alloys on copper substrates is governed by the atomic affinity towards copper and the probability of close atomic contact at the interface.[45] To further elucidate this phenomenon, the phase composition of the liquid metal after interaction with the H62 electrode was characterized by using SEM coupled with EDS. As shown in Fig. S3, residual liquid metal micro-regions were observed on the H62 surface after HCl treatment. EDS mapping (see Fig. S3b–f) and line scans (Fig. S3g) revealed the presence of Zn within these liquid metal regions, indicating that Zn atoms had diffused from the H62 electrode into the liquid metal at room temperature. Therefore, this process transforms the interface into a Ga–In–Zn ternary liquid system. Similar diffusion–dissolution behaviors in Ga–In–Zn ternary liquid metals have been documented previously.[46,47] Analysis of the Cu–Zn and Cu–Ga phase diagrams reveals distinct interaction pathways. According to the solvus thermodynamics and recent findings,[37,42,48] Zn preferentially dissolves into the liquid Ga phase rather than forming solid Cu–Zn intermetallics at the interface. Consequently, the H62 interface is characterized by concurrent $CuGa_2$ formation and Zn leaching, the latter of which poses long-term embrittlement risks.

Consequently, solid–liquid interface interactions strongly influence the electrical contact resistance. Improved wettability at the interface enhances electrical contact quality, significantly reducing contact resistance. Recent studies indicate that Zn alloying in copper reduces the contact angle with EGaIn, promoting rapid spreading. However, this chemical interaction poses a severe risk of liquid metal embrittlement (LME). As demonstrated by Ezequiel *et al.*, copper–zinc alloys with high Zn content (usually >20%) undergo a ductile-to-brittle transition under long-term exposure to EGaIn, leading to catastrophic intergranular fracture under stress.[42] Given that H62 brass contains approximately 38% Zn, it is inherently susceptible to this failure mode. The dissolution of Zn into the liquid metal not only alters the interface chemistry but also significantly compromises the electrode's mechanical integrity over time. In contrast, pure copper (T2) has been proven to be resistant to LME, maintaining ductile failure modes even in prolonged contact with gallium-based alloys.[49] While the formation of the $CuGa_2$ intermetallic layer on T2 leads to a slower stabilization of contact resistance compared to H62, it creates a mechanically robust interface that does not suffer from environmentally assisted cracking. Therefore, for practical applications requiring long-term reliability and structural

safety, T2 copper is the superior choice, whereas H62 should be restricted to non-load bearing, short-term interconnects.

To evaluate the potential for practical application, the total resistance was measured using planar T2 and H62 electrodes (dimensions: 50 × 0.5 × 0.2 mm) under the following three conditions: (1) when filled with liquid metal, (2) when filled with an electrical compound grease (Kunlun 801 power grease), and (3) when left unfilled (control). The surfaces of all copper-based electrodes were pre-treated with 1 M HCl to remove contaminants and promote reactive wetting. The inset in Fig. 5a illustrates the four-wire method used to measure the total resistance of each sample. To ensure consistent and reliable measurements, standardized pressure was applied to the overlapping regions of the electrodes. This was achieved by placing a 150 g weight on the overlap, which maintained stable and uniform contact.

As shown in Fig. 5a, using the liquid metal as the electrical contact material resulted in a total resistance significantly lower than that of the conventional T2–T2 direct crimp connection (4.01 mΩ). When employing electrical compound grease, the total resistance decreased, but not significantly. Specifically, the total resistance of the T2–EGaIn–T2 connection filled with EGaIn was as low as 1.79 mΩ, representing a reduction of 2.22 mΩ. H62 electrodes exhibited a similar trend (as shown in Fig. 5b), with the total resistance of H62 electrode connections being higher than that of T2 due to the greater resistivity of H62. The total resistance of the H62–EGaIn–H62 connection filled with EGaIn was 6.96 mΩ, which is a reduction of 2.12 mΩ compared to the H62–H62 crimp connection (9.08 mΩ). Consequently, using the liquid metal as an electrical interface material effectively reduces contact resistance and ensures stable electrical connections. This further highlights the significant effectiveness of the solid–liquid reaction wetting strategy in minimizing interface resistance in electrical connections.

In practical applications, using the gallium-based liquid metal as an electrical interface material between solid electrodes can effectively reduce contact resistance. For the H62 electrode, for example, Zn atoms diffuse from the substrate into the gallium-based liquid metal, thereby enhancing interfacial interactions. However, prolonged exposure to the gallium-based liquid metal can degrade the structural integrity of the H62 electrode itself, suggesting that it is more suitable for short-term electrical contacts involving such liquid metals. In contrast, the stable $CuGa_2$ intermetallic layer formed at the T2–EGaIn interface enables durable and reliable electrical connections, making T2 electrodes preferable for long-term solid–liquid contact scenarios.

4. Conclusions

This study provides a systematic evaluation of the electrical contact between four different cylindrical copper alloys (T2, H62, QSn6.5-0.1, C15760) and liquid metal, revealing that different types of copper electrodes can affect reactive wetting and electrical contact stability. The wettability between the four copper-based electrodes and the gallium-based liquid metal differs. The formation of a $CuGa_2$ intermetallic compound layer on the electrode surface markedly promotes wetting, resulting in a significant reduction in the solid–liquid contact resistance. Prolonged contact further facilitates the interfacial reaction, continuously improving wettability and reducing contact resistance. Of all the tested electrodes, the T2 and H62 electrodes exhibited the lowest contact resistance, demonstrating superior electrical contact performance. Compared to conventional solid–solid mechanical crimp connections, using a liquid metal electrical interface material effectively reduces contact resistance and enables more stable and reliable electrical connections. These results highlight the significant application potential of gallium-based liquid metal for advanced power electronics and flexible interconnects.

Author contributions

Jiasheng Zu: investigation, experimentation, data processing, and writing; Yuntao Cui: writing, experimentation, data processing, review, and editing; Chunwei Li: investigation and data processing; Xueqing Chen: investigation; Zhongshan Deng: conceptualization, writing, review, and editing.

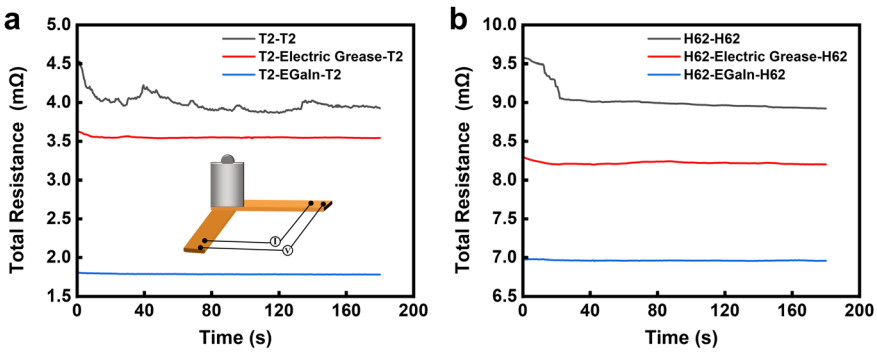

Fig. 5 Total resistance of two copper-based electrodes under different contact conditions: (a) T2 and (b) H62.

Conflicts of interest

The authors declare no competing financial interests.

Data availability

The data supporting this article have been included as part of the supplementary information (SI). Supplementary information: the SI includes a discussion of the transmission line model (TLM), surface and cross-sectional morphologies of copper-based electrodes (SEM images), contact resistance measurements and fitted curves, EDS surface mapping and line scan analyses, and physical properties of the electrodes. See DOI: https://doi.org/10.1039/d5lf00370a.

Acknowledgements

The research was supported by the Key Research Program of the State Key Laboratory of Cryogenic Science and Technology (Grant No. E5ASR20201).

References

1 G. Wu, K. Dong, Z. Xu, S. Xiao, W. Wei, H. Chen, J. Li, Z. Huang, J. Li, G. Gao, G. Kang, C. Tu and X. Huang, *Railw. Eng. Sci.*, 2022, **30**, 437–467.
2 Y. Song and W. Xiao, *Infrastructures*, 2024, **9**, 110.
3 X. Wang, H. Li, R. Yao, H. Long, Y. Zhong, R. Yu and J. Li, presented in part at the 2019 IEEE 21st Electron. Packag. Technol. Conf. (EPTC), 2019.
4 D. C. Miller, R. L. Arnold, P. L. Hacke, C.-S. Jiang, S. C. Hayden, H. Moutinho, J. M. Newkirk, G. Perrin, L. T. Schelhas, K. Terwilliger, S. Ulicna and C. Xiao, *IEEE J. Photovolt.*, 2024, **14**, 793–802.
5 K. Sawa, Y. Watanabe, T. Ueno and H. Masubuchi, *IEICE Trans. Electron.*, 2020, **E103-C**, 705–712.
6 X. Lafontan, C. Dufaza, M. Robert, F. Pressecq and G. Perez, presented in part at the Des., Test, Integr. Packag. MEMS/MOEMS 2001, 2001.
7 J. W. McBride and H. Liu, presented in part at the Proc. 2020 IEEE 66th Holm Conf. Electr. Contacts, 2020.
8 J. P. Kumar, *Materials*, 2018, **11**, 1010.
9 M. J. Brand, P. A. Schmidt, M. F. Zaeh and A. Jossen, *J. Energy Storage*, 2015, **1**, 7–14.
10 R. Wang, L. Xu and Y. Zhou, *J. Electr. Comput. Eng.*, 2021, **2021**, 5514674.
11 Q. Wang, Y. Yu and J. Liu, *Adv. Eng. Mater.*, 2018, **20**, 1700781.
12 Q. Zhuang, K. Yao, C. Zhang, X. Song, J. Zhou, Y. Zhang, Q. Huang, Y. Zhou, X. Yu and Z. Zheng, *Nat. Electron.*, 2024, **7**, 1–12.
13 Y. Lin, T. Fang, C. Bai, Y. Sun, C. Yang, G. Hu, H. Guo, W. Qiu, W. Huang, L. Wang, Z. Tao, Y. Lu and D. Kong, *Nano Lett.*, 2023, **23**, 11174–11183.
14 Y. Wu, L. Huang, X. Huang, X. Guo, D. Liu, D. Zheng, X. Zhang, R. Ren, D. Qu and J. Chen, *Energy Environ. Sci.*, 2017, **10**, 1854–1861.
15 J. Ye, Y. Yao, J. Gao, S. Chen, P. Zhang, L. Sheng and J. Liu, *Soft Rob.*, 2022, **9**, 1098–1107.
16 C. Li, M. Qiao, H. Zhang, Y. Zhou, J. Liu, L. Wang and Z. Deng, *Adv. Eng. Mater.*, 2024, **26**, 2400090.
17 F. Polo-Garzon, Z. Wu, Y. Li, J. Zhang, X. Yu, E. Toups, E. Lopez-Honorato, J. T. Damron, J. C. Foster, Y. Cheng, L. L. Daemen, A. J. Ramirez-Cuesta and H. M. Meyer, *Sci. Adv.*, 2024, **10**, eadm9963.
18 W. Xiang, J. Ye, Z. Xing, P. Zhang, X. Chen, L. Wang and J. Liu, *ACS Appl. Electron. Mater.*, 2023, **5**, 6003–6013.
19 R. Yuan, Y. Cao, X. Zhu, X. Shan, B. Wang, H. Wang, S. Chen and J. Liu, *Adv. Mater.*, 2024, **36**, 2309182.
20 M. Choi, J. Kim, S. Kim, H. Koo and J. So, *Adv. Funct. Mater.*, 2024, **34**, 2310318.
21 X. Zhang, Z. Deng, H. Song, M. Guo and L. Li, *Sci. China Mater.*, 2024, **67**, 3976–3985.
22 K. B. Ozutemiz, J. Wissman, O. B. Ozdoganlar and C. Majidi, *Adv. Mater. Interfaces*, 2018, **5**, 1701596.
23 C. Li, M. Qiao, J. Su, Q. Wang, H. Zhang, L. Wang and Z. Deng, *ACS Appl. Electron. Mater.*, 2024, **6**, 8513–8524.
24 D. K. Sarfo, R. R. Taylor and A. P. O'Mullane, *ACS Appl. Electron. Mater.*, 2020, **2**, 2921–2928.
25 J. B. Andrews, K. Mondal, T. V. Neumann, J. A. Cardenas, J. Wang, D. P. Parekh, Y. Lin, P. Ballentine, M. D. Dickey and A. D. Franklin, *ACS Nano*, 2018, **12**, 5482–5488.
26 D. Gutierrez, J. Alejandro de Sousa, M. Mas-Torrent and N. Crivillers, *ACS Appl. Electron. Mater.*, 2020, **2**, 3093–3099.
27 M. Kim, J. J. Park, C. Cho and S. H. Ko, *Adv. Funct. Mater.*, 2023, **33**, 2303286.
28 Y. G. Park, Y. W. Kwon, C. S. Koh, E. Kim, D. H. Lee, S. Kim, J. Mun, Y. M. Hong, S. Lee, J. Y. Kim, J. H. Lee, H. H. Jung, J. Cheon, J. W. Chang and J.-U. Park, *Nat. Commun.*, 2024, **15**, 3394.
29 T. Sato and E. Iwase, presented in part at the 2023 IEEE 36th Int. Conf. Micro Electro Mech. Syst. (MEMS), 2023.
30 T. Sato and E. Iwase, *ACS Appl. Mater. Interfaces*, 2023, **15**, 44404–44412.
31 S. Kim, D. Jeong, J. Oh and J. Bae, presented in part at the 2019 2nd IEEE Int. Conf. Soft Rob. (RoboSoft), 2019.
32 L. Kogut and K. Komvopoulos, *J. Appl. Phys.*, 2003, **94**, 3153–3162.
33 G. K. Reeves and H. B. Harrison, *IEEE Electron Device Lett.*, 1982, **3**, 111–113.
34 R. Holm, *Electric Contacts: Theory and Application*, Springer, 4th edn, 1967.
35 Y. Chen, C. Liu, Z. Zhou and C. Liu, *J. Manuf. Process.*, 2022, **84**, 1310–1319.
36 Y. Chen, H. Jiang, Z. Zhou and C. Liu, *Mater. Today Commun.*, 2024, **38**, 108401.
37 Z. Gao, C. Wang, Z. Chai, Y. Chen, C. Shen, K. Yao, N. Zhao, Y. Wang and H. Ma, *Mater. Chem. Phys.*, 2022, **282**, 125960.
38 S. Liu, S. McDonald, Q. Gu, S. Matsumura, D. Qu, K. Sweatman, T. Nishimura and K. Nogita, *J. Electron. Mater.*, 2020, **49**, 128–139.
39 Y. Cui, F. Liang, Z. Yang, S. Xu, X. Zhao, Y. Ding, Z. Lin and J. Liu, *ACS Appl. Mater. Interfaces*, 2018, **10**, 9203–9210.
40 J. Tang, X. Zhao, J. Li, Y. Zhou and J. Liu, *Adv. Sci.*, 2017, **4**, 1700024.

41 G. Sang, X. Zhang, W. Li, Y. Li, Y. Chen, X. Zhang, H. Song, Y. Cui and Z. Deng, *J. Mater. Chem. C*, 2026, **14**, 1940–1948.
42 M. Ezequiel, I. P. Serre, T. Auger, E. Heripre, Z. Hadjem-Hamouche and L. Perriere, *Eng. Failure Anal.*, 2024, **164**, 108694.
43 S. Guo, C. Wang, L. Wang, Z. Chai, Y. Chen, H. Ma, Y. Wang and Z. Gao, *J. Mater. Sci.: Mater. Electron.*, 2023, **34**, 11017.
44 P. Protsenko, A. Terlain, V. Traskine and N. Eustathopoulos, *Scr. Mater.*, 2001, **45**, 1439–1445.
45 S. Kulawik, W. Gierlotka, A. Debski, W. Gasior and A. Zajaczkowski, *J. Mol. Liq.*, 2021, **325**, 115114.
46 S. Knott, C. Chen, F. Gehringer and A. Mikula, *Int. J. Mater. Res.*, 2006, **97**, 1102–1107.
47 Z. Zhao, S. Soni, T. Lee, C. A. Nijhuis and D. Xiang, *Adv. Mater.*, 2023, **35**, 220391.
48 X. Du, W. Wang, Z. Ding, X. Wang, Y. Qiao, S. Wei, Q. Zhu and J. Guo, *J. Mater. Sci.: Mater. Electron.*, 2023, **34**, 10782.
49 M. Ezequiel, I. P. Serre and A. Fadel, *Metals*, 2025, **15**, 1194.